Intelligent System for Automated Spheroid Segmentation Using Machine Learning

Intelligent Health Systems – From Technology to Data and Knowledge
E. Andrikopoulou et al. (Eds.)

doi:10.3233/SHTI250399

Intelligent System for Automated Spheroid Segmentation Using Machine Learning

Alessandra INTROVAIA[a,1], Andrea BEZZE[b], Sara MUCCIO[b], Clara MATTU[b], and Gabriella BALESTRA[a]
[a] *Department of Electronics and Telecommunications – Politecnico di Torino, Italy*
[b] *Department of Mechanical and Aerospace Engineering – Politecnico di Torino, Italy*
ORCiD ID: Alessandra Introvaia https://orcid.org/0009-0003-6526-7697
ORCiD ID: Andrea Bezze https://orcid.org/0000-0002-8061-5034
ORCiD ID: Sara Muccio https://orcid.org/0009-0002-1757-7597
ORCiD ID: Clara Mattu https://orcid.org/0000-0002-3969-8771
ORCiD ID: Gabriella Balestra https://orcid.org/0000-0003-2717-648X

Abstract. Image segmentation is a crucial task of medical image processing, including the analysis of multicellular tumour spheroids (MTSs), a common *in vitro* model used in cancer research for drug screening. Accurate segmentation of MTSs images allows the extraction of the morphological features necessary for the evaluation of the efficacy of the treatment they undergo. This paper presents an artificial intelligence (AI)-based segmentation system for the analysis of RGB images of MTS using machine learning (ML) classifiers. Unlike previous methods designed for high-performance microscope images, our system focuses on RGB images captured by standard bench-top optical microscopes, offering a cost-effective and accessible solution for research. The preliminary results demonstrate the efficacy of the ML approach in achieving the desired outcome.

Keywords. Multicellular spheroids, In vitro models, Image segmentation, Artificial Intelligence, Machine Learning

1. Introduction

The success rate of translating nanomedicines from experimental research to clinical trials is less than 30% [1]. Consequently, preclinical validation systems must ensure rapid and reliable screening for high-throughput evaluation. Multicellular tumour spheroids (MTSs) are widely used *in vitro* models for preclinical drug screening in cancer research [2]. These three-dimensional, non-adherent cell aggregates typically consist of heterogeneous cell populations and can be tailored to replicate the physiological spatial structure of tumours like glioblastoma multiforme (GBM). This flexibility makes them valuable for studying tumour biology and drug screening. Nevertheless, colorimetric viability tests, commonly used to assess drug effects on MTSs, are expensive, time-consuming, and destructive, prompting the need for alternatives. In this context, optical microscopy has gained attention as a label-free method for evaluating treatment efficacy [3]. MTSs volume and morphological features, such as circularity and invasion area, are strongly linked to cell viability, making them more effective for assessing drug response

[1] Corresponding Author: Alessandra Introvaia; E-mail: alessandra.introvaia@polito.it.

[2]. However, due to variability in MTSs preparation, numerous optical images are needed to extract key data for monitoring treatment outcomes.

Hence the quality and speed of image segmentation are crucial for the accurate determination of these metrics. To enhance segmentation and parameter extraction, robust and reliable image processing algorithms are necessary. Automated methods are taking over the field of image processing due to their ability to address common challenges, such as the time-consuming, operator-dependent nature of the process, and limited scalability. Among these new proposals, *Chen et al.* [4] introduced *SpheroidSizer,* a MATLAB-based tool for MTSs segmentation using a Chan-Vese level-set algorithm. This tool allows for the extraction of quantitative parameters like area, width, length, and volume. Similarly*, Akshay et al.* [5] presented a user-friendly Deep Learning (DL) tool for MTSs image analysis, named *SpheroScan*, which is based on a ResNet-50 feature pyramid network as a backbone. These algorithms target high-performance microscope images, limiting their applicability for RGB images from standard optical microscopes.

This paper aims to bridge this gap by presenting the preliminary results of a method for the automatic segmentation of RGB images of MTSs using Machine Learning (ML) classifiers. This approach is designed to provide an accessible and cost-effective solution for images captured by these widely used microscopes in preclinical research.

2. Methods

2.1. Dataset

In this study, a dataset of RGB images of MTSs was acquired through optical microscopy. GBM MTSs were prepared in low adhesion conditions using a combination of GBM cells (U87) and GBM-associated stem cells (GMB-8), with other cells of the TME, such as microglia (HMC3) and astrocytes (HASTR), to replicate tumour histology. Briefly, cells were seeded in an Ultra-Low Attachment 96-wells Plate (Corning) (4000 cells/well) in the following ratios: 63% U87, 7% GBM-8 cells, 30 % HASTR (TMH) and 63% U87, 7% GBM-8 cells, 15 % HASTR, 15% HMC3 (BioMix). Plates were incubated at 37°C for 4 days to allow the maturation of MTSs. Then, MTSs were treated with different concentrations (10, 20, 50, 100, 200, 500 nM) of Bortezomib-loaded nanoparticles, as described in previous studies [6]. Untreated MTSs were used as control. To assess the impact of the treatment, images of each MTS were captured at four time steps (0, 24, 48, and 72 hours) using a Leica DMi1 Optical Microscope.

The analysis was conducted on 20 MTSs of the BioMix composition and 21 of the TMH composition, yielding a total of 164 images. Each 24-bit RGB image had a resolution of 1824x1368 pixels. Segmentation was performed on each image by a researcher through the auto-detection algorithm of the NIS Elements Advanced Research software (Nikon), which creates a region of interest (ROI) from the borders of an object within the image. The ROI were then manually adjusted by the operator and the resulting masks were used as a reference.

2.2. Dataset division

In order to develop a segmentation system based on AI methods, it is first necessary to divide the initial dataset into two distinct subsets: the Construction Set (CS), employed for the construction of the AI model, and the Test Set (TS), which is utilized to ensure

the model's generalisation ability. The division was based on the analysis of the key characteristics of the images (i.e., mean value and standard deviation of the area to be segmented). Hierarchical clustering [7] was employed to construct a dendrogram, to highlight potential patterns in the data, both across the entire dataset and separately for the two cellular compositions. Since no significant distinguishing patterns were observed, a random sampling from the clusters identified in the dendrogram was performed, maintaining an 80% ratio for the CS and 20% for the TS. This process resulted in the creation of a CS consisting of 131 images and a TS with 33 images.

2.3. Segmentation methods

2.3.1. AI system construction

The AI-based segmentation system was developed through a series of steps applied exclusively to the images within the CS. All this pipeline has been implemented on Python 3.10. Initially, all images underwent pre-processing, where they were converted to grey-scale and subsequently normalised using the min-max scaling technique, which was performed to reduce the variability across the images.

Subsequently, the regions of interest (ROIs) were identified and labelled using a sliding window approach with a fixed window size of 50x50 pixels for each image, with a 50% overlap between adjacent windows. As the segmentation relies on supervised learning, the ROIs were labelled according to their respective gold standard masks. Specifically, regions were classified as background (label 0) if at least 90% of their pixels belonged to the background, or as spheroid (label 1) if at least 80% of the pixels were part of the segmented object.

Afterwards, features were extracted using the PyRadiomics package [8]. For each ROI, both the first-order features (i.e., histogram-based) and the secondo-order texture features derived from the Gray Level Co-Occurrence Matrix (GLCM), were computed [9]. To ensure all features were on a comparable scale, they were normalised through min-max scaling, bringing their values into the range of [0,1].

The CS was then divided into Training Set (TRS) and Validation Set (VS), by applying a random sampling with a 70% to 30% ratio. The TRS was employed to train various ML classifiers, while the VS was used for the fine-tuning of parameters. Due to the imbalance in the dataset, where class 0 ROIs (background) were significantly more numerous than class 1 ROIs (spheroid), under-sampling was applied to the background class in order to obtain a balanced TRS.

At this point, several classifiers, including k-Nearest Neighbours (k-NN), Multi-Layer Perceptron (MLP), Random Forest (RF), and eXtreme Gradient Boosting (XGBoost), were trained and their performance evaluated using accuracy as the primary evaluation metric. The segmented masks were then reconstructed by aggregating the classification results of individual ROIs, using their respective coordinates, and applying majority voting to define the class in overlapping regions. The quality of the segmentations was quantified using metrics such as Dice similarity coefficient, Jaccard index, precision and recall computed with the corresponding gold standard masks.

2.3.2. AI system validation

In order to evaluate the generalisation capability of the ML model, all the steps of the pipeline were repeated on the TS data. Specifically, the feature normalisation was

conducted by considering the minimum and maximum values of the features computed on the CS data.

3. Results

Figure 1 presents the boxplots of the Dice, Jaccard, Precision and Recall metrics evaluated for the AI-based segmentation system for both the CS and the TS data. These results were obtained using an MLP classifier with the following configuration: two hidden layers with sizes equal to twice the number of input features and equal to the number of input features, respectively, an alpha value of 0.001, a learning rate of 0.001, and the ReLU activation function. It can be noticed that the median values for all the computed metrics were relatively high, demonstrating consistent overlap between the automated segmentations and the ground truth. Overall, the distribution of metrics between the TS and CS datasets was similar, highlighting the model's robust generalisation capabilities.

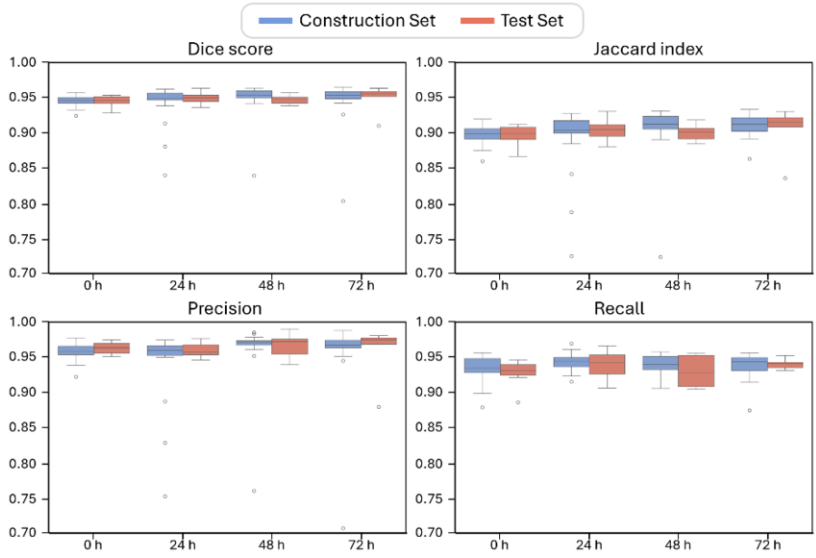

Figure 1. Boxplots of Dice sore, Jaccard index, Precision and Recall for CS and TS computed.

Figure 2 shows the results of the segmentation of the *BioMix 20nM 3* spheroid across the four time-steps that were analysed. The contours displayed include both the automatic contours obtained through the AI segmentation system and the reference contours. It can be observed that the automatic contours are characterised by how the ROIs were identified, resulting in contours that vary in size by 50x50 pixels. Overall, the automatic contours appear to closely align with the reference contours, demonstrating the effectiveness of the proposed method in capturing the spheroid's morphology.

4. Conclusions

This paper presents the findings of the application of an AI segmentation system to 164 images of 41 different spheroids. The results demonstrate that the system achieves

satisfactory segmentation accuracy, with consistent performance across both the Construction and Test sets. However, there are limitations that require further investigation. Firstly, the current dataset is relatively limited and homogeneous, which may limit the generalisability of the model. Secondly, the ROIs size may reduce segmentation accuracy in cases where greater detail is required. Future works will focus on refining the segmentation process by reducing the ROIs size and incorporating post-processing steps to achieve more precise segmentations.

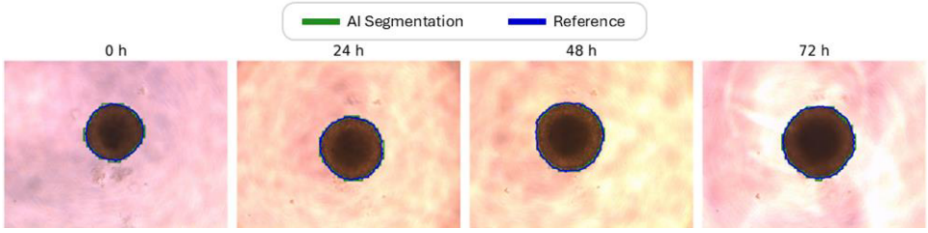

Figure 2. Segmentation results of the BioMix 20nM 3 spheroid over time-steps.

Acknowledgments

The research scholarship of Alessandra Introvaia is supported by the project POC NAPTER NODES which has received funding from the MUR – M4C2 1.5 of PNRR funded by the European Union - NextGenerationEU (Grant agreement no. ECS00000036). Sara Muccio acknowledges “JUST THE WOMAN I AM 2023” for founding her research fellowship.

References

[1] Takebe T, Imai R, Ono S. The Current Status of Drug Discovery and Development as Originated in United States Academia: The Influence of Industrial and Academic Collaboration on Drug Discovery and Development. Clin Transl Sci. 2018 Nov;11(6):597-606. doi: 10.1111/cts.12577.

[2] Ivanov DP, Parker TL, Walker DA, et al. Multiplexing Spheroid Volume, Resazurin and Acid Phosphatase Viability Assays for High-Throughput Screening of Tumour Spheroids and Stem Cell Neurospheres. PLoS ONE 2014 Aug 9(8): e103817. doi:10.1371/journal.pone.0103817

[3] Costa EC, Moreira AF, de Melo-Diogo D, et al. 3D tumor spheroids: an overview on the tools and techniques used for their analysis. Biotechnol Adv. 2016 Dec;34(8):1427–41, doi: 10.1016/j.biotechadv.2016.11.002

[4] Chen W, Wong C, Vosburgh E, Levine AJ, Foran DJ, Xu EY. High-throughput Image Analysis of Tumor Spheroids: A User-friendly Software Application to Measure the Size of Spheroids Automatically and Accurately. JoVE. 2014 Jul 8;(89):51639, doi: 10.3791/51639.

[5] Akshay A, Katoch M, Abedi M., et al. SpheroScan: a user-friendly deep learning tool for spheroid image analysis. GigaScience. 2022 Dec 28;12:giad082, doi: 10.1093/gigascience/giad082

[6] Mattu C, Brachi G, Menichetti L, et al. Alternating block copolymer-based nanoparticles as tools to modulate the loading of multiple chemotherapeutics and imaging probes. Acta Biomaterialia. 2018; 80:341-351, doi: 10.1016/j.actbio.2018.09.021.

[7] Nielsen F. Introduction to HPC with MPI for Data Science. Cham: Springer International Publishing; 2016. doi: 10.1007/978-3-319-21903-5

[8] Van Griethuysen, JJ, Fedorov A, Parmar C, et al. Computational Radiomics System to Decode the Radiographic Phenotype. Cancer Research. 2017 Nov 1;77(21):e104–7. doi: 10.1158/0008-5472.CAN-17-0339

[9] Mayerhoefer ME, Materka A, Langs G, Häggström I, Szczypiński P, Gibbs P, et al. Introduction to Radiomics. J Nucl Med. 2020 Apr;61(4):488–95. doi: 10.2967/jnumed.118.222893